Combined Surface-Enhanced Infrared Spectroscopy and First-Principles Study on Electro-Oxidation of Formic Acid at Sb-Modified Pt Electrodes

Bin Peng, Hui-Fang Wang, Zhi-Pan Liu,* and Wen-Bin Cai*

Shanghai Key Laboratory of Molecular Catalysis and Innovative Materials and Department of Chemistry, Fudan University, Shanghai 200433, China

Received: November 3, 2009; Revised Manuscript Received: January 21, 2010

In situ electrochemical surface-enhanced infrared absorption spectroscopy (EC-SEIRAS) together with a periodic density functional theory (DFT) calculation has been initially applied to investigate the mechanism of formic acid electro-oxidation on Sb-modified Pt (Sb/Pt) electrode. EC-SEIRAS measurement reveals that the main formic acid oxidation current on Sb/Pt electrode is ca. 10-fold enhanced as compared to that on clean Pt electrode, mirrored by nearly synchronous decrease of the CO and formate surface species, suggesting a "non-formate" oxidation as the main pathway on the Sb/Pt electrode. On the basis of the calculations from periodic DFT, the catalytic role of Sb adatoms can be rationalized as a promoter for the adsorption of the CH-down configuration but an inhibitor for the adsorption of the O-down configuration of formic acid, kinetically facilitating the complete oxidation of HCOOH into CO_2. In addition, Sb modification lowers the CO adsorption energy on Pt, helps to mitigate the CO poisoning effect on Pt.

1. Introduction

With a relevance to the anode reaction of direct formic acid fuel cell (DFAFC), intensive investigations have been conducted to elucidate the mechanism of HCOOH (FA) electro-oxidation at Pt-based surfaces.[1–15] A "dual pathway" mechanism was proposed that consists of the "direct" pathway and "CO-intermediate" pathway.[1–3,5,6,11,12] Modification of a Pt surface with a secondary metallic adlayer like Sb[6,16–21] is considered to be an efficient way to hinder the "CO-intermediate" pathway, by taking advantage of the so-called "third-body effect" and/or "electronic effect",[20] in addition to the use of Pt-based alloys and intermetallics.[22–25] In fact, the Sb-modified Pt/C catalyst has been used in practical DFAFC, yielding significant improvement in overall cell performances.[19,21] Mechanistic understanding of FA electro-oxidation on Sb-modified Pt (simplified hereafter as Sb/Pt) may provide useful clues for searching and designing new efficient Pt-based catalysts.

Conventional external infrared reflection absorption spectroscopy (IRAS) had been applied to investigate the oxidation of FA in the earlier studies,[4,7,17,26–31] and Yang et al.[17] first reported FA electro-oxidation with IRAS on Sb/Pt(110) electrode. Unfortunately, due to the extremely low surface sensitivity of their IRAS, only the CO_L band is identified and thus is unable to provide a deep insight into FA electro-oxidation on Sb/Pt electrode. Notably, in situ attenuated-total-reflection surface-enhanced infrared absorption spectroscopy (ATR-SEIRAS) has merits of high surface sensitivity and unrestricted mass transport, facilitating real-time measurements. With ATR-SEIRAS, surface formate species was observed at ca. 1322 cm^{-1} during FA electro-oxidation on unmodified Pt electrode.[11–14] Samjeské et al. ascribed this formate species to the active intermediate for the dominant reaction pathway.[11] In contrast, Chen et al. suggested a "triple pathway" mechanism in which the formate species was assigned to the intermediate of the additional minor pathway, that is, "formate pathway", rather than to that of the major "direct" pathway.[13,14] Since the electrochemistry of FA oxidation on a Pt electrode is significantly changed in the presence of Sb adatom modification, it remains unclear either dual- or triple- pathway mechanism may better apply for FA electro-oxidation on this practically important Sb/Pt electrode.

In addition to surface spectroscopic analysis, the DFT calculation is regarded as an important complementary tool for structural and mechanistic study in surface electrochemistry.[32,33] On the basis of the DFT calculations, Neurock et al. showed that the FA molecule could decompose via an experimentally undetectable *COOH intermediate which has very low energy barrier for its further transformation to CO_2.[34] Recently, Wang and Liu reported DFT calculations of FA oxidation on Pt(111)/H_2O interface with a continuum solvation model.[35] They showed that the presence of formate promoted the adsorption of FA in a CH-down configuration, which is a reactive precursor leading to CO_2. Importantly, both calculations by Neurock et al. and Wang et al. showed that the adsorbed formate species was rather stable and difficult to be decomposed to CO_2. Therefore, the increase of the CH-down adsorption configuration is the key to increase the electrocatalytic oxidation of FA on Pt electrode. To the best of our knowledge, no relevant DFT calculations have been available to elucidate the mechanism of the superior oxidation current of FA on Sb/Pt electrode.

In the present study, real-time EC-SEIRAS in conjunction with periodic DFT calculations have been extended for the mechanistic study of the FA electro-oxidation on Sb/Pt electrode for the first time. The results by these two different methods are in reasonable agreement, which suggests a "non-formate" direct oxidation pathway involving the enhanced CH-down adsorption configuration of formic acid on Sb/Pt electrode surface.

2. Experimental Section

2.1. Preparation of Sb/Pt Electrodes. The Pt electrode for electrochemical ATR-SEIRAS was prepared on the total-reflecting plane of a hemicylindrical Si prism via the so-called "two-step" wet process in which a 60 nm thick Au chemically

* To whom correspondence should be addressed. E-mail: (W.-B.C.) wbcai@fudan.edu.cn; (Z.-P.L.) zpliu@fudan.edu.cn. Fax: +86-21-65641740.

10.1021/jp910497n
Published on Web 02/01/2010

deposited on Si followed by subsequent electrodeposition of a 5 nm thick pinhole-free Pt overlayer.[36] The Sb/Pt (θ_{Sb} = ca. 0.6) electrode was prepared by electrodeposition of Sb at 0.5 V (vs reversible hydrogen electrode (RHE)) for 15 min in 0.5 M H_2SO_4 solution containing 0.1 mM antimony potassium tartrate (APT) followed by electrodesorpiton of partial Sb at 0.72 V (vs RHE) for 30 min in another 0.5 M H_2SO_4 solution.[16] Note that the θ_{Sb} for the Sb modified Pt film electrode is defined as the ratio of filled and unfilled Pt sites, evaluated from the UPD hydrogen sorption charges of Pt electrode in the absence and the presence of Sb modification. Also noted is that this θ_{Sb} could be overestimated. In contrast, much smaller values were also reported for saturated Sb coverages on Pt(111) (0.38),[37] Pt(110) (0.37),[17] and Pt(100) (0.33)[37] based on the charge under the sharp oxidation peak of Sb_{ad} on single crystal Pt surfaces. Unfortunately, no such clear sharp oxidation peak can be found on our Pt film electrode, making it difficult to estimate the Sb coverage based on the latter method.[19] In the following, the UPD H adsorption/desorption charge method is used for the evaluation of Sb on Pt film electrode.

Electrochemical control was achieved with a CHI 605B electrochemistry workstation (CH Instruments, Shanghai) in deaerated 0.5 M H_2SO_4 with and without 0.1 M HCOOH. After the Pt electrode was electrochemically cleaned, HCOOH was injected into the electrolytic cell at 0.1 V (vs RHE) and mixed by bubbling Ar for another 200 s before the initiation of measurements. The as-prepared Sb/Pt electrode served as the working electrode with a Pt sheet as the counter electrode. An RHE was used as the reference electrode to avoid the interference of Cl^- and all potentials are cited with respect to this RHE. The otherwise same electrochemical ATR-SEIRAS measurement except in 0.5 M $HClO_4$ instead of 0.5 M H_2SO_4 was also conducted for comparison, and the results are shown in the Supporting Information.

Details of electrochemical ATR-SEIRAS have been described elsewhere.[11,36] Briefly, a Varian 3100 FTIR spectrometer equipped with a liquid-nitrogen cooled MCT detector was operated at a resolution of 8 cm^{-1} with an acquisition time of 0.2 s for each spectrum in the real-time spectroelectrochemical measurement. All the spectra in this paper are shown in the absorbance units defined as $A = -\log(I/I_0)$, where I and I_0 represent the intensities of the reflected radiation at the sample and reference potentials, respectively. All measurements were performed at room temperature (20 ± 2 °C).

2.2. DFT Calculation Setups. All calculations were carried out based on the periodic DFT calculations with ultrasoft pseudopotentials[38] with plane-wave basis sets.[39,40] A plane-wave cutoff of 400 eV was used. The exchange-correlation functional applied was at the generalized gradient approximation level, known as GGA-PBE. The Pt(111) surface was modeled by a four-layer rectangular ($4 \times 2\sqrt{3}$) slab with the top two layers relaxed. A vacuum spacing of 15 Å was used and all adsorbates were placed on one side of the slab. All Sb atoms were initially put at the face-centered cubic hollow sites of the Pt(111), which is the most stable adsorption site.

3. Results and Discussion

3.1. Realtime EC-SEIRAS on Pt and Sb/Pt Electrodes. Series of SEIRA spectra for a Pt electrode recorded simultaneously with the cyclic voltammogram at 10 mV s^{-1} are shown in Figure 1. The spectrum recorded at 1.3 V was used as the reference. The bands at 2052−2073 and 1810−1845 cm^{-1} can be assigned to linear- and bridge-bonded CO, denoted as CO_L and CO_B, respectively. The 1320 cm^{-1} band comes from

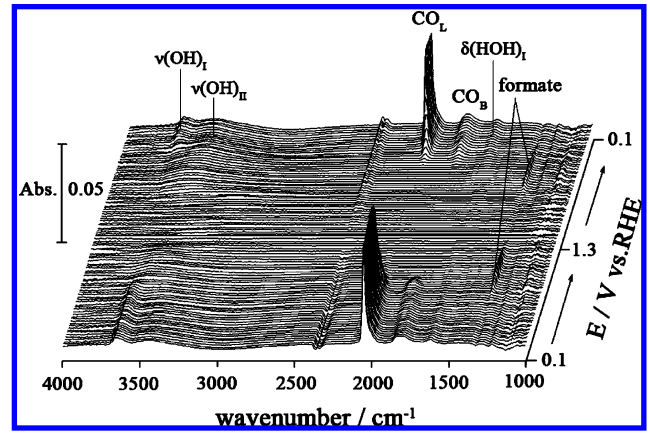

Figure 1. Series of time-resolved SEIRAS spectra of the unmodified Pt electrode surface acquired during the cyclic voltammetry at 10 mV s^{-1} in 0.5 M H_2SO_4 + 0.1 M HCOOH solution. The reference spectrum was taken at 1.3 V.

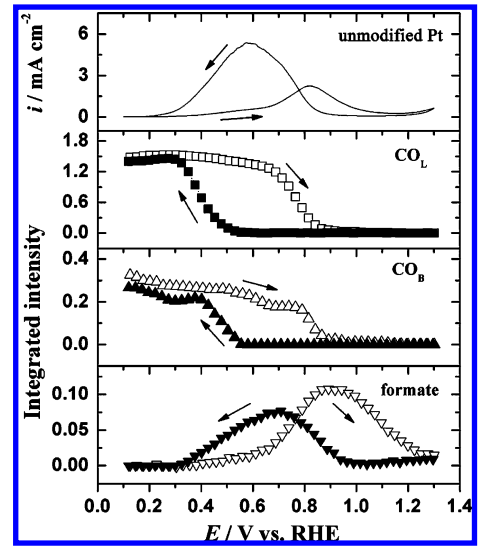

Figure 2. Selected integrated intensities of CO_L, CO_B, and formate on Pt surface during cyclic voltammetry. Data were taken from Figure 1.

symmetric O−C−O stretching of formate species bridge-adsorbed on Pt.[11,13,14,41] The band at 3650 cm^{-1} can be assigned to OH stretching mode ($\nu(OH)_I$) of the surface free H_2O coexisted with CO[36] with its counterpart band at 1630 cm^{-1} to HOH bending mode ($\delta(HOH)_I$). The bands around 3450 and 1220 cm^{-1} come from outer layers of interfacial water ($\nu(OH)_{II}$) and (bi) sulfate from the electrolyte side, respectively, and the noisy absorption around 1130 cm^{-1} is due to the low transmittance of the Si prism. The obtained spectra on the Pt electrode resembles those obtained on chemically deposited Pt electrode.[11,13,14]

Figure 2 shows integrated intensities of the CO_L, CO_B, and formate bands adapted from Figure 1 as a function of potential. On the positive potential scan, the intensity of CO_L slightly increases at the beginning due to the partial conversion from CO_B to CO_L[11] and decreases substantially at ca. 0.7 V, corresponding to the CO oxidation. A very small anodic current was observed at potentials lower than 0.4 V, mirrored by the intense CO bands (resulted from self-dissociation of FA on Pt) and the invisible formate band. The formate band intensity showed up at ca. 0.4 V and peaked at ca. 0.85 V in response to an anodic current peak due to the releasing of fresh Pt sites by CO oxidation. On the negative scan, the formate band intensity reaches the maximum again at ca. 0.65 V together with a high

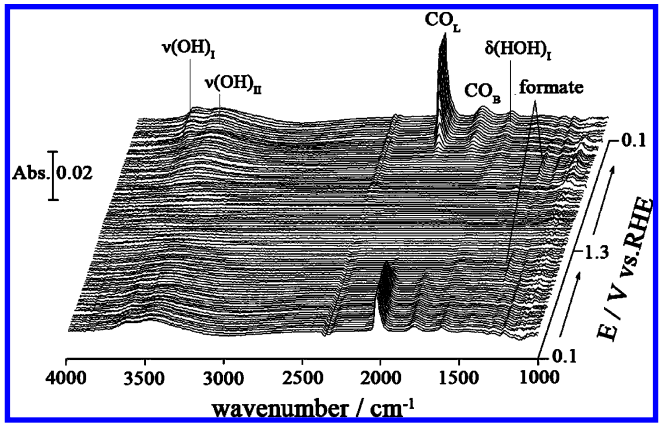

Figure 3. Series of time-resolved SEIRAS spectra of the Sb/Pt (θ_{Sb} = 0.6) electrode surface. Details of the definition of θ_{Sb} could be found in the experimental section. The experimental conditions are the same as that in Figure 1.

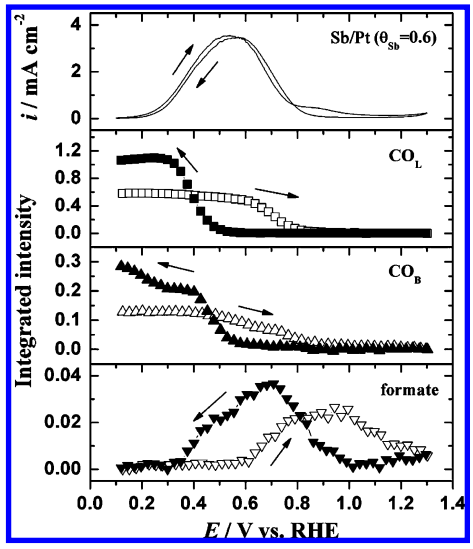

Figure 4. Selected integrated band intensities for CO_L, CO_B, and formate on Sb/Pt electrode during cyclic voltammetry. Data were taken from Figure 3.

anodic current peak, then it decreases rapidly when CO readsorbs at ca. 0.55 V due to the decomposition of FA. Because of this apparently synchronized relationship between the formate band intensity and the anodic current, Samjeské et al. proposed that formate was the intermediate of the direct pathway.[11] Also noted is that Chen et al. compared the chronoamperometric transients with formate band intensities under different FA concentrations.[13,14] A formate pathway was suggested besides the direct and "indirect" pathways based on the nonlinear relationship between the oxidation current and the formate band intensity. Nevertheless, the relationship is not necessarily linear if a second order reaction kinetics with formate may be involved.[11]

The bands of CO_L, CO_B, formate, (bi)sulfate, interfacial, and free water can also be seen for the corresponding realtime EC-SEIRAS measurement on the Sb/Pt electrode as shown in Figures 3 and 4. As compared to those in Figure 1, reduction of the band intensities is obvious. Specifically, the CO_L band gives a much smaller intensity at the beginning of positive scan with Sb modification, and it reverts to larger values at lower potentials in the negative scan after the electrodesorption of Sb at more positive potentials. The most interesting feature in Figure 4 is that the formate band intensity is hardly seen until 0.6 V in the positive scan regardless of the greatly enhanced oxidation current centered on ca. 0.5 V. This observation clearly demonstrates that the formate coverage is not an essential or a key factor contributing to the anodic current at least on Sb/Pt electrode. In fact, at 0.5 V in the positive potential scan, the oxidation current for FA is increased by ca. 10-fold on Sb/Pt electrode as compared to that on Pt electrode, accompanied with the decrease of formate band intensity by ca. 4 fold. Considering that CO oxidation on Sb/Pt electrode at potentials up to ca. 0.6 V is trivial if any as deduced from the potential dependent CO band intensity, the "indirect CO-intermediate" pathway can be essentially excluded. Therefore, the enhanced FA electro-oxidation currents on Sb/Pt electrode at lower anodic potentials should mainly result from the direct reaction pathway.

On the other hand, the anodic current at 0.55 V is nearly the same either in the positive or negative scan in Figure 4. Much higher surface formate coverage is observed in the latter due to the absence of CO and desorption of Sb at more positive potentials. This higher coverage of preadsorbed formate on Pt(111) could promote the direct pathway via the C−H down adsorption of FA before they are swiftly converted to CO_2 based on our previous periodic DFT calculations,[35] thus may account for the observed high oxidation current in the backward scan even with the loss of Sb modification. As the potential sweeps more negatively, CO starts to accumulate on the surface and formate starts to be desorbed from the surface, leading to decreased current. The above postulation may also be applied to explain qualitatively the similar result in Figure 2. Moreover, the oxidation of FA on Pt and Sb/Pt is also investigated in $HClO_4$ solution. The obtained results are in general similar to those obtained in H_2SO_4 solution, especially as far as the main oxidation of HCOOH in the positive scan is concerned (see Supporting Information). On the basis of these results, it may be concluded that the current strategy of combined electrochemical SEIRAS and first-principles study is valid in understanding the enhanced electrocatalysis on Sb/Pt electrode.

EC-SEIRAS measurement reveals that the modification of Sb resulted in not only enhanced current but also decreased CO and formate. However, the decrease of the formate coverage may negatively contribute to the electro-oxidation of FA no matter what the formate species was regarded as a reactive intermediate[11] or as the promoter for the formation of FA CH-down adsorption.[35] Although the decreased coverage of CO by half is beneficial to the enhanced current, it seems insufficient to account for the great enhancement in electrocatalysis of Sb/Pt. To justify the Sb effect on the above puzzling issues, in the following we will utilize periodic DFT calculations of the FA and CO adsorption on both clean Pt(111) and Sb-covered Pt(111) (Sb/Pt(111)) surfaces to help understand the above observations.

3.2. Periodic DFT Calculations of FA Adsorption on Sb/Pt(111) Surfaces. Using DFT, we then calculated the adsorption of formic acid on both clean Pt(111) and various Sb-covered Pt(111) (Sb/Pt(111)) surfaces as shown in Figure 5a−d. No attempt was made to simulate the electrochemical potentials directly since it was shown that the variation of the electric field of electrodes has little direct effect on the formic acid adsorption and reactions, but the local coverage of the surface species that affected by the electrochemical potentials is more important.[35] Following our previous calculations on clean Pt(111), four explicit water molecules were always included to simulate the core solvation shell of formic acid in solution, giving rise to a HCOOH-$(H_2O)_4$ complex.[35] Two different adsorption configurations of HCOOH-$(H_2O)_4$ have been identified, namely the CH-down configuration and the O-down

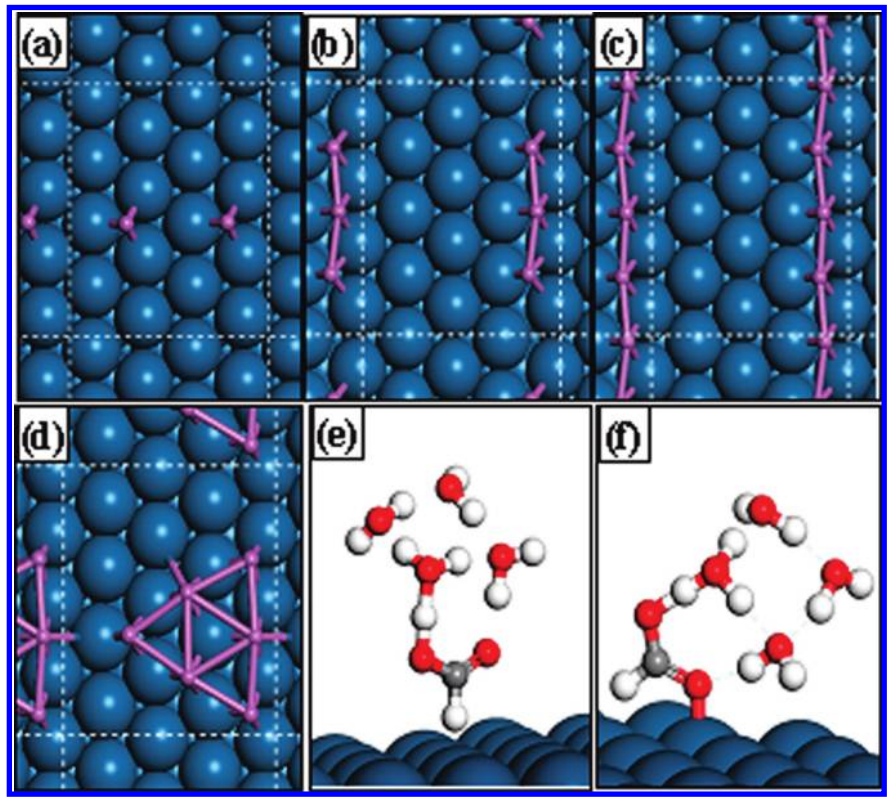

Figure 5. The Sb/Pt(111) model systems and the adsorption of formic acid on the surfaces. (a) Adatom model at 0.125 ML; (b) 1D-chain Sb/Pt(111) model at 0.187 ML; (c) 1D-chain Sb/Pt(111) model at 0.25 ML; (d) 2D-island Sb/Pt(111) model at 0.375 ML; (e) the CH-down configuration of formic acid (HCOOH-(H2O)$_4$) adsorption on Pt(111); (f) the O-down configuration of formic acid adsorption on Pt(111).

TABLE 1: The Calculated Adsorption Energies (E_{ads}) and the Proportion (P%, at 300 K) of the Formic Acid in the CH-down Configuration and the O-down Configuration on Clean Pt(111) and Sb Covered Surfaces[a]

species		pure Pt(111)	adatom (0.125 ML)	1D chain (0.187 ML)	1D chain (0.25 ML)	2D-island (0.375 ML)
HCOOH-$(H_2O)_4$(CH-down)	E_{ads}/eV(P%)	−0.02(∼0)	−0.14(0.18))	−0.14(26)	−0.14(32)	−0.12(99.99)
HCOOH-$(H_2O)_4$(O-down)	E_{ads}/eV(P%)	−0.32(∼100)	−0.30(99.82)	−0.17(74)	−0.16(68)	0.20(<0.01)
CO	E_{ads}/eV	−1.66	−1.62	−1.48	−1.41	−1.36

[a] The E_{ads} of CO is also listed.

configuration, as shown in Figure 5e,f, respectively (only the optimized structures on clean Pt(111) were shown for the purpose of illustration). In the CH-down configuration, the H of the CH bond points directly toward the top of one surface Pt atom, while in O-down configuration the O-atom of carbonyl group attaches to a surface Pt atom forming a O−Pt bond.

The adsorption energy (E_{ads}) of HCOOH-$(H_2O)_4$ is defined as the energy change due to the adsorption, which is the difference between the DFT total energy of the adsorbed HCOOH-$(H_2O)_4$ system and the sum of the energies of the clean substrate and the gas-phase HCOOH-$(H_2O)_4$ complex. The adsorption of HCOOH-$(H_2O)_4$ on the Sb sites of the Sb/Pt(111) systems has first been studied and it was found that both adsorption configurations of formic acid are much less stable than their counterparts on the Pt sites. This implies that the surface Sb coverage on Pt(111) should not be too high, since sufficient exposed Pt sites are essential for the decomposition of formic acid. Indeed, this agrees well with previous experimental results, which showed a "volcano-shape" dependence of electrocatalysis on θ_{Sb}.[16,17,20]

The calculated E_{ads} of HCOOH-$(H_2O)_4$ at Pt sites on clean Pt(111) and different Sb/Pt(111) systems are listed in Table 1. Table 1 shows that the O-down configuration is more stable than the CH-down configuration on Pt(111) by 0.30 eV. In the presence of Sb atoms on the Pt(111), it is generally found that the O-down configuration is destabilized as compared to it on the pure Pt(111), while the CH-down configuration is stabilized. In particular, when the Sb coverage increases to 0.375 ML in a 2D island, the O-down configuration can no longer adsorb due to the endothermic nature of the adsorption (+0.20 eV). By contrast, the adsorption energy of the CH-down configuration is rather constant with the increase of surface Sb coverage. According to the adsorption energy, it is possible to determine the proportion of the two configurations on the surfaces at 300 K with the Boltzmann distribution law. The calculated values are also listed in Table 1. It shows that the O-down configuration remains dominant on the surface when Sb coverage is less than 0.25 ML. As the Sb coverage is 0.375 ML in a 2D island configuration, the CH-down configuration becomes the dominant species on the surface.

On the basis of our previous work,[35] the O-down configuration of formic acid is the precursor for the production of formate on Pt(111), which is however difficult to degrade at the metal/solution interface kinetically, while the CH-down configuration is the key reaction precursor leading to the complete oxidation of formic acid into CO_2. Therefore, the catalytic role of Sb in this work can be rationalized as a promoter for the adsorption of the CH-down configuration but an inhibitor for the adsorption

TABLE 2: The Calculated Bader Net Charge (Q) of the Adsorbed Sb and the Adsorbed HCOOH-$(H_2O)_4$ on the Clean Pt(111), 1D Chain Sb/Pt(111) (0.25 ML), 2D Island Sb/Pt(111) (0.375 ML)

Q(|e|)	pure Pt(111)	1D chain (0.25 ML)	2D island (0.375 ML)
Sb	0	+0.52	+0.55
HCOOH-$(H_2O)_4$(CH-down)	+0.03	−0.02	−0.03
HCOOH-$(H_2O)_4$(O-down)	+0.19	−0.03	−0.07

of the O-down configuration. This conclusion reconciles the experimental observations shown in Figure 1−4 that (i) the detected formate band intensity is obviously decreased on Sb-modified Pt electrodes as compared to the unmodified electrodes, and (ii) the oxidation current of formic acid electro-oxidation is greatly enhanced on Sb-modified electrodes at potentials when a very low formate band is detected, that is, 0.1−0.6 V in the positive-going scan.

We also studied the adsorption of CO on Sb/Pt(111) surfaces since CO is generally believed to be a poisoning species on Pt catalysts in electrocatalytic oxidation of FA, which can only be oxidized at higher potentials. The adsorption energies of CO on the top site of Pt are also listed in Table 1. It is found that CO adsorption is weakened by about 0.2−0.3 eV due to the addition of Sb. It indicates that Sb helps to relieve the CO poisoning of Pt catalysts, which is in good agreement with the experimental observations that the detected CO band intensity is greatly reduced on the Sb-modified Pt electrodes (Figure 3 and 4) as compared to the unmodified electrodes (Figure 1 and Figure 2). However, it does not necessarily mean that the stripping of a predosed CO adlayer on Sb/Pt electrode should occur at a more negative potential as compared to that on Pt electrode, since the electrooxidation of a CO adlayer depends not only on the CO adsorption strength but also on the coverage and structure of CO adlayer as well as on the availability of the reactive oxygen-containing species (see Supporting Information).[42]

To further understand why Sb can affect the adsorption configuration of HCOOH-$(H_2O)_4$ on Pt, we have carried out a detailed Bader charge analysis on the adsorbed model systems. The Bader charge here is defined to be the electronic charge enclosed within the Bader volume developed by the Richard Bader's theory of atoms in molecules (AIM).[43,44] The Bader net charge (Q) is the difference between the calculated Bader charge and the electronic charge of the neutral atom. The results on the adsorbed HCOOH-$(H_2O)_4$ are listed in Table 2. As shown in Figure 5e,f, the HCOOH-$(H_2O)_4$ is a highly polarized complex with a negative end $[HCOO]^{\delta-}$ and a solvated proton-like end $[H_9O_4]^{\delta+}$ forming a HCOO−H−$(H_2O)_4$ linkage. The δ equals to 0.7 |e| for the gas-phase HCOOH-$(H_2O)_4$. When this complex adsorbs on Pt(111) in O-down configuration, electrons (about 0.19 e) flow from the O atoms of the $[HCOO]^{\delta-}$ end to the surface Pt atoms via the O−Pt bond, thus leading to the negatively charged Pt sites. This contributes to the high stability of O-down configuration at the clean Pt(111) surface. In the CH-down configuration, by contrast, no significant charge transfer occurs, which is consistent with the low adsorption on the clean Pt(111), only about −0.02 eV.

On going to the Sb/Pt(111) surfaces, for example, the 1D chain- and 2D island-modeled Sb/Pt(111), we found that the net charge of each Sb atom is about +0.5 |e| on average, and the Pt surface is strongly negatively charged. The charge transfer leads to a strong surface dipole normal to the surface plane. This dipole can couple well with the intrinsic dipole of the HCOOH-$(H_2O)_4$ complex in the CH-down configuration, where the HCOO−H−$(H_2O)_4$ linkage is normal to the surface plane (Figure 5e). The dipole−dipole interaction stabilizes the CH-down configuration. By contrast, such a dipole−dipole coupling is largely reduced when the HCOOH-$(H_2O)_4$ complex adsorbs via the O-down configuration because the HCOO−H−$(H_2O)_4$ linkage of the O-down configuration (Figure 5f) is not normal to the surface plane. On the other hand, the electron transfer from Sb to Pt weakens the electron transfer ability from the O atoms to the surface Pt atoms. Therefore, the O-down configuration becomes less stable on the Sb-covered Pt(111) surfaces as compared to that the clean Pt(111) as calculated by DFT shown in Table 1.

4. Conclusion

In summary, electro-oxidation of FA on Sb/Pt electrode has been investigated by EC-SEIRAS and periodic DFT calculation. The EC-SEIRAS reveals that greatly enhanced anodic current at lower potentials with Sb on Pt electrodes mirrored by the significantly decreased CO band intensity and the extremely weakened formate band intensity, suggesting that the enhanced electro-oxidation of FA mainly proceeds via the non-formate direct pathway at Sb/Pt electrode.

Periodic DFT calculations shows that the presence of Sb on Pt(111) promotes the adsorption of formic acid via a CH-down configuration, in which the CH-bond has a direct contact with active Pt sites. This configuration was known to be the precursor to CO_2 and responsible for the major oxidation current. The theoretical results explain the enhanced anodic current of FA electro-oxidation on Sb/Pt electrodes even when a negligible amount of bridged formate was detected. From Bader charge analysis, the addition of Sb on Pt causes a surface dipole of $[Sb]^{\delta+}$-$[Pt]^{\delta-}$, which contributes to the enhanced adsorption of CH-down configuration via electrostatic interaction. Besides, DFT calculation also confirms that CO adsorption is weakened on Sb/Pt(111) surfaces, indicating that the addition of Sb to Pt can help to relieve the CO poisoning on Pt electrodes. The combined electrochemical ATR-SEIRAS and first-principles study may be generally extended to the investigation of electrocatalytic oxidation of FA on other efficient adatom-modified Pt surfaces.

Acknowledgment. This work is supported by the NSFC (20873031, 20833005, 20673027 for W.B.C. and 20825311, 20773026 for Z.P.L.) and the STCSM (08JC1402000, 08DZ2270500).

Supporting Information Available: Stripping voltammograms for CO-predosed Pt and Sb/Pt electrodes and electrochemical ATR-SEIRAS results for formic acid oxidation on these two electrodes in $HClO_4$ solutions. This material is available free of charge via the Internet at http://pubs.acs.org.

References and Notes

(1) Breiter, M. W. *J. Electroanal. Chem.* **1967**, *14*, 407.
(2) Capon, A.; Parsons, R. *J. Electroanal. Chem.* **1973**, *44*, 1.
(3) Parsons, R.; VanderNoot, T. *J. Electroanal. Chem.* **1988**, *257*, 9.
(4) Chang, S. C.; Leung, L. W. H.; Weaver, M. J. *J. Phys. Chem.* **1990**, *94*, 6013.
(5) Markovic, N. M.; Gasteiger, H. A.; Ross, P. N.; Jiang, X. D.; Villegas, I.; Weaver, M. J. *Electrochim. Acta* **1995**, *40*, 91.
(6) Kizhakevariam, N.; Weaver, M. J. *Surf. Sci.* **1994**, *310*, 183.

(7) Iwasita, T.; Xia, X. H.; Herrero, E.; Leiss, H. D. *Langmuir* **1996**, *12*, 4260.
(8) Lu, G. Q.; Crown, A.; Wieckowski, A. *J. Phys. Chem. B* **1999**, *103*, 9700.
(9) Okamoto, H.; Kon, W.; Mukouyama, Y. *J. Phys. Chem. B* **2004**, *108*, 4432.
(10) Chen, Y. X.; Ye, S.; Heinen, M.; Jusys, Z.; Osawa, M.; Behm, R. J. *J. Phys. Chem. B* **2006**, *110*, 9534.
(11) Samjeské, G.; Miki, A.; Ye, S.; Osawa, M. *J. Phys. Chem. B* **2006**, *110*, 16559.
(12) Samjeské, G.; Osawa, M. *Angew. Chem., Int. Ed.* **2005**, *44*, 5694.
(13) Chen, Y. X.; Heinen, M.; Jusys, Z.; Behm, R. J. *Angew. Chem., Int. Ed.* **2006**, *45*, 981.
(14) Chen, Y. X.; Heinen, M.; Jusys, Z.; Behm, R. J. *Langmuir* **2006**, *22*, 10399.
(15) Uhm, S.; Lee, H. J.; Lee, J. *Phys. Chem. Chem. Phys.* **2009**, *11*, 9326.
(16) Watanabe, M.; Horiuchi, M.; Motoo, S. *J. Electroanal. Chem.* **1988**, *250*, 117.
(17) Yang, Y. Y.; Zhou, Z. Y.; Sun, S. G. *J. Electroanal. Chem.* **2001**, *500*, 233.
(18) Fernandez-Vega, A.; Feliu, J. M.; Aldaz, A.; Claviller, J. *J. Electroanal. Chem.* **1989**, *258*, 101.
(19) Peng, B.; Wang, J. Y.; Zhang, H. X.; Lin, Y. H.; Cai, W. B. *Electrochem. Commun.* **2009**, *11*, 831.
(20) Leiva, E.; Iwasita, T.; Herrero, E.; Feliu, J. M. *Langmuir* **1997**, *13*, 6287.
(21) Lee, J. K.; Jeon, H.; Uhm, S.; Lee, J. *Electrochim. Acta* **2008**, *53*, 6089.
(22) Tripković, A. V.; Popović, K. Dj.; Stevanović, R. M.; Socha, R.; Kowal, A. *Electrochem. Commun.* **2006**, *8*, 1492.
(23) Bauer, J. C.; Chen, X. L.; Liu, Q. S.; Phan, T. H.; Schaak, R. E. *J. Mater. Chem.* **2008**, *18*, 275.
(24) Matsumoto, F.; Roychowdhury, C.; DiSalvo, F. J.; Abruña, H. D. *J. Electrochem. Soc.* **2008**, *155*, B148.
(25) Miura, A.; Wang, H. S.; Leonard, B. M.; Abruña, H. D.; DiSalvo, F. J. *Chem. Mater.* **2009**, *21*, 2661.
(26) Beden, B.; Bewick, A.; Lamy, C. *J. Electroanal. Chem.* **1983**, *148*, 147.
(27) Kunimatsu, K. *J. Electroanal. Chem.* **1986**, *213*, 149.
(28) Sun, S. G.; Claviler, J.; Bewick, A. *J. Electroanal. Chem.* **1988**, *240*, 147.
(29) Kitamura, F.; Takahashi, M.; Ito, M. *Surf. Sci.* **1989**, *223*, 493.
(30) Lamy, C.; Léger, J. M. *J. Chim. Phys.* **1991**, *88*, 1649.
(31) Gómez, R.; Weaver, M. J. *J. Electroanal. Chem.* **1997**, *435*, 205.
(32) Delgado, J. M.; Rodes, A.; Orts, J. M. *J. Phys. Chem. C* **2007**, *111*, 14476.
(33) Delgado, J. M.; Blanco, R.; Orts, J. M.; Pérez, J. M.; Rodes, A. *J. Phys. Chem. C* **2009**, *113*, 989.
(34) Neurock, M.; Janik, M.; Wieckowski, A. *Faraday Discuss.* **2008**, *140*, 363.
(35) Wang, H. F.; Liu, Z. P. *J. Phys. Chem. C* **2009**, *113*, 17502.
(36) Yan, Y. G.; Li, Q. X.; Huo, S. J.; Ma, M.; Cai, W. B.; Osawa, M. *J. Phys. Chem. B* **2005**, *109*, 7900.
(37) Jung, G.; Park, H.; Rhee, C. K. *J. Electroanal. Chem.* **1998**, *453*, 243.
(38) Vanderbilt, D. *Phys. Rev. B* **1990**, *41*, 7892.
(39) Kresse, G.; Hafner, J. *J. Phys.: Condens. Matter* **1994**, *6*, 8245.
(40) Kresse, G.; Hafner, J. *Phys. Rev. B* **1994**, *49*, 14251.
(41) Xue, X. K.; Wang, J. Y.; Li, Q. X.; Yan, Y. G.; Liu, J. H.; Cai, W. B. *Anal. Chem.* **2008**, *80*, 166.
(42) Marković, N. M.; Ross, P. N. *Surf. Sci. Rep.* **2002**, *45*, 117.
(43) Bader, R. *Atoms in Molecules: A Quantum Theory*; Oxford University Press: New York, 1999.
(44) Sanville, E.; Kenny, S. D.; Smith, R.; Henkelman, G. *J. Comput. Chem.* **2007**, *28*, 899.

JP910497N